Analysis of the Characteristics of a Synchronous Generator by means of Air Gap Flux

AUTHOR(S):

MATSUKI, Junya; OKADA, Takao

CITATION:

MATSUKI, Junya ...[et al]. Analysis of the Characteristics of a Synchronous Generator by means of Air Gap Flux. Memoirs of the Faculty of Engineering, Kyoto University 1985, 47(3): 205-219

ISSUE DATE:

1985-08-15

URL:

http://hdl.handle.net/2433/281301

Analysis of the Characteristics of a Synchronous Generator by means of Air Gap Flux

By

Junya MATSUKI* and Takao OKADA*

(Received March 30, 1985)

Abstract

This paper describes the analysis of the characteristics of a synchronous generator on the basis of air gap fluxes measured by a search coil on the stator tooth top. It is especially concerned with the loss of synchronism process which governs the stability of an electric power system, but has not yet been made clear physically. That is to say, the principles of measuring air gap flux by using a search coil, methods of determining direct axis positions, derivation of no-load air gap flux density distribution, derivation of armature reaction flux, and the analysis of the loss of synchronism process are described.

This is a modified paper of our previous works[1,2] which is aimed at giving a total understanding of the physical behavior of a synchronous generator connected to an electric power system, over the wide range of operations from the sready-state to the step-out process. This will contribute to the efforts of both the design engineers of electrical apparatus and the power system engineers.

1 INTRODUCTION

In the design of synchronous machines it is important to determine the air gap flux accurately. The finite element method[3] or finite difference method[4] has been applied recently, and has provided more detailed and exact information than the previous graphical method[5]. Also, for the power system stability, more realistic and accurate models for the machine have been developed and used for stability calculation. These calculation methods based on the mathematical models are very effective, but require tedious accumulation of numerical data, and the results are frequently not consistent with the real phenomena. Although great emphasis is now placed on the mathematical analysis, we need to consider the air gap flux rather than the voltage and the equivalent reactance to deal with the internal physical behavior upon which the machine actually operates.

So we measured the air gap flux of a synchronous generator directly by search

* Department of Electrical Engineering.

coils and analyzed the physical behaviors in the air gap. The changes of the flux waveforms and the reasons for those waveforms were investigated physically. For the first time, we succeeded in being able to give physical descriptions of the loss of synchronism process, and to clarify the relation between the behavior of air gap flux and the stability of the synchronous machine.

In a recent paper[6], search coils were used for checking the values of magnetic induction obtained numerically. Such usage has been familiar in many investigations. This type of research reported in our paper has not been published yet.

2 FLUX MEASUREMENT BY MEANS OF SEARCH COILS

This section describes the model generator, the principles of measuring the air gap flux by using search coils, the selection of search coils used in this analysis and the methods of determining direct axis postitions.

2.1 Model Generator

The three-phase synchronous ganerator used is of a four salient pole type and has a rated capacity of 6kVA, rated voltage 220V, rated current 15.7A, rated power factor 0.9 and rated speed 1,800 rpm.

The synchronous generator has search coils for measurement of fluxes at every part of rotor and stator. Stator search coils used are arranged as shown in Fig. 1. These search coils are wound at seven positions (from No. 1 through No. 7) in each pair of tooth and slot. Eight sets of the seven coils (three turns each) are arranged at

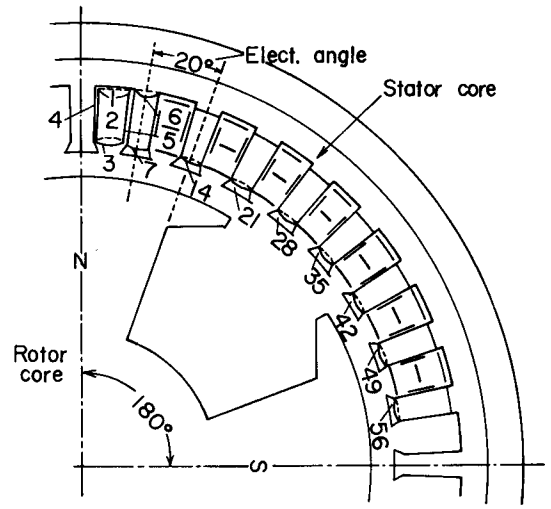

Fig. 1 Position of search coils

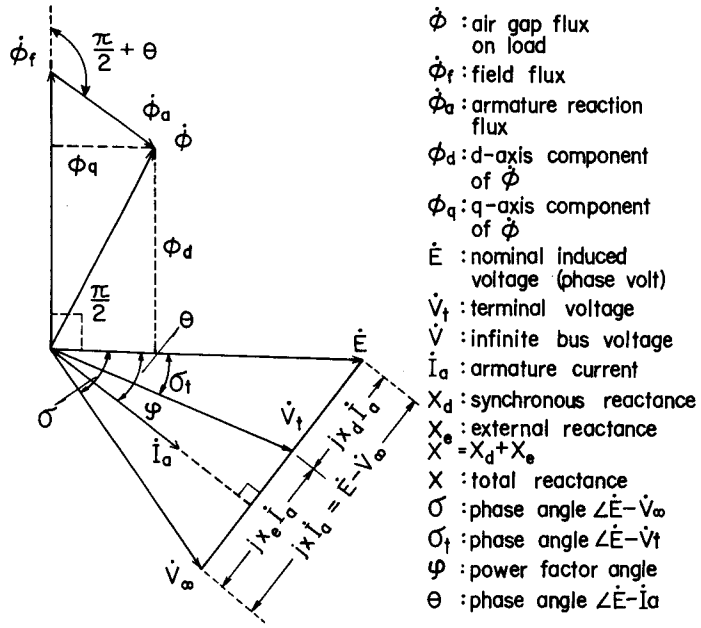

Fig. 2 Phasor diagram

a 20° electrical angle.

Fig. 2 shows the phasor diagram of a synchronous generator.

2.2 Measurement Principles

The induced voltage e_i of a search coil mounted on the armature shown in Fig. 1 is expressed in the following equation.

$$e_i = -N_i(d\phi_i/dt) \tag{1}$$

where i is the search coil number, N_i is the turns of a search coil and ϕ_i is the flux interlinked with the search coil.

From this induced voltage e_i, flux ϕ_i interlinked with each search coil may be found as follows.

$$\phi_i = -\frac{1}{N_i}\int e_i dt \tag{2}$$

Flux measurement and data processing can be done in the following way. The search coil's induced voltage waveform is recorded by a data recorder (TEAC model R-280). This data is given to the computer and the flux waveform is obtained by numerical integration. The sampling time interval is 0.125 ms. The search coil

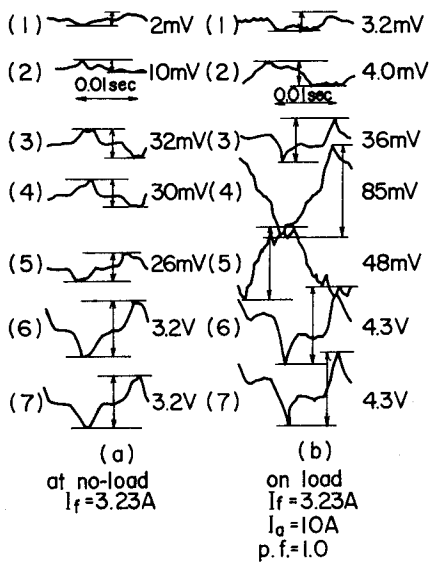

Fig. 3 Induced voltages of every search coil No. 1–No. 7

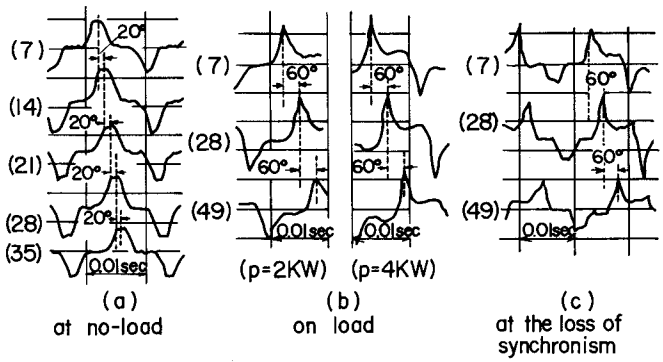

Fig. 4 Induced voltages of each search coil and their phase relasions

current is less than 1 μA and its effect can be ignored.

2.3 Selection of Search Coils

In Fig. 1, the search coils No. 1 through No. 7 measure the following flux.

(1) The slot internal flux is measured by search coils No. 1, No. 2 and No. 3.

(2) The slot wall flux, which passes through the slot wall, is measured by search coils No. 4 and No. 5.

(3) The tooth core internal flux, which passes through the inside of the tooth core,

is measured by search coils No. 6 and No. 7.

Fig. 3 (a) shows the induced voltage of each search coil with the field current 3.23 A which generates no-load rated voltage. The voltages of the search coils (1), (2), (3) are very small. The flux at the slot inlet (3) is approximately 1/100 as compared with that of (7). Therefore, it is clear that almost all of the air gap flux at no-load passes through the tooth top of the armature core.

Next, the induced voltage of each coil on load is shown in Fig. 3 (b). The slot internal flux is very little like that at no-load, but the slot wall flux by (4) increases. This flux is part of the armature coil leakage flux and its value is dependent on load current.

Judging from the above, the tooth top of the stator is most suitable as the position of search coils for measuring the air gap flux.

Next, induced voltages of every search coil (see Fig. 1, No. 7, 14, 21, 28 and 35) on the stator tooth top at no-load have been measured as shown in Fig. 4 (a). In addition, in a one-machine connected to an infinite bus system, the induced voltages of search coils No. 7, 28 and 49 at the steady state are shown in Fig. 4 (b), and at the loss of synchronism they are shown in Fig. 4 (c).

Under any condition, the induced voltage waveforms of each search coil are almost equal in all respects, and the phase differences are 20° or 60° in electrical angle, which is identical to the interval of search coils. Consequently, the air gap flux measurement need not have all the above search coils. Any of these search coils on the stator tooth top can be represented for the purpose. The analysis in this paper is based on the search coil No. 7.

2.4 Determination of Direct Axis

It is important to determine accurately the location of the direct axis in the

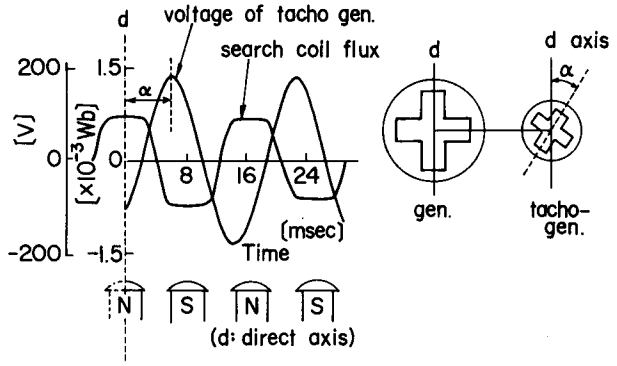

Fig. 5 Determination of the direct axis of the flux distribution

analysis of the characteristics of the synchronous generator. As shown in Fig. 5, the direct axis is determined from the center of the trapezoidal flux waveform obtained by the search coil at no-load. (See the next section.) By the phase angle between the direct axis and the voltage of a tacho-generator, the direct axis position at any load operation can be determined.

3 ANALYSIS OF THE AIR GAP FLUX

3.1 Derivation of No-load Air Gap Flux Distribution

When a generator is operated at no-load, at rated speed and the field current is 3.23 A, the induced voltage waveform of search coil No. 7 is shown in Fig. 6 (a), while the flux waveform given by a numerical integration of this voltage is shown in Fig. 6 (b). The flux waveform by this search coil is of a trapezoidal form and contains the second harmonic component 1.0% of the fundamental wave, the third harmonic 18.3%, the fourth harmonic 0.4%, the fifth harmonic 2.5%, the sixth harmonic 0.1% and the seventh harmonic 0.6%, respectively. Since the armature core and gap permeance

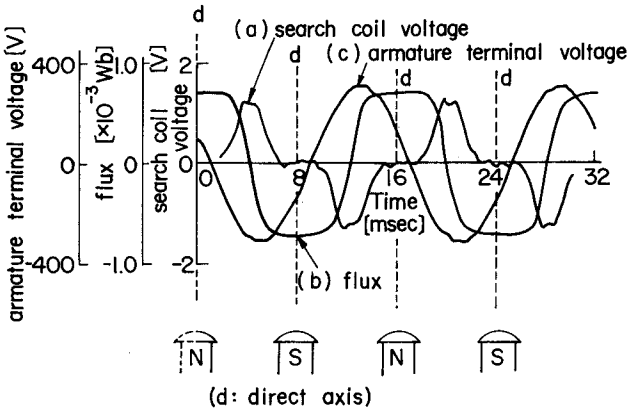

Fig. 6 Flux waveform at no-load

Table 1 Comparison of odd harmonics of flux ϕ via the search coil and air gap flux density distribution B

Harmonics	1	3	5	7	Harmonics/Fundamental %		
					3	5	7
ϕ_k[×10⁻³Wb]	2.511	0.459	0.063	0.015	18.28	2.51	0.60
B_k[Wb/m²]	1.110	0.203	0.028	0.007	18.29	2.52	0.63

are symmetrical with respect to the axis of the field pole, even harmonic components are almost all negligibly small, Also, higher harmonic components than the seventh are negligible. Therefore, the flux waveform by the search coil is mainly composed of the fundamental wave component and the third harmonic component. This flux waveform by means of the search coil may be considered as the air gap flux (density) distribution as stated below.

In the synchronous generator which rotates at no-load at synchronous speed ω_o, where the axis of the field pole is set as zero point, the air gap flux density distribution B at x point from the zero point is expressed by the following equation.

$$B = \sum_{k=1}^{\infty} B_k \cos\left\{k(\omega_o t - \frac{\pi}{\tau}x)\right\} \qquad (Wb/m^2) \tag{3}$$

where k: order of harmonics, τ: 0.216 m (pole pitch).

The total flux ϕ which interlinks with the search coil is calculated by the following equation:

$$\begin{aligned}\phi &= \int_{-\delta/2}^{\delta/2} N\ell B dx \\ &= N\ell \sum_{k=1}^{\infty}\left[\left\{\frac{2\tau}{k\pi}\cdot\sin(\frac{k\pi}{2\tau}\delta)\right\}\cdot B_k \cos k\omega_o t\right] \qquad (Wb)\end{aligned} \tag{4}$$

where N is the number (3) of winding turns of the search coil, ℓ is the length of search coil's axial direction (0.13 m) and δ is the width 0.0058 m of the search coil.

On the other hand, the flux ϕ is also found from the induced voltage e of the search coil.

$$\phi = -\int e dt = \sum_{k=1}^{\infty} \phi_k \cos k\omega_o t \qquad (Wb) \tag{5}$$

Equations (4) and (5) are equal so that the following equation is obtained.

$$B_k = \phi_k / \left\{N\ell \cdot \frac{2\tau}{k\pi}\cdot\sin(\frac{k\pi}{2\tau}\delta)\right\} \qquad (Wb/m^2) \tag{6}$$

$$(k = 1, 2, \cdots\cdots)$$

Therefore, the air gap flux density distribution B may be found by substituting the harmonics ϕ_k of ϕ into Eq. (6) and then Eq. (3). Table 1 shows a comparison of the odd harmonics of ϕ and B. The harmonics of both waveform agree well. Consequently, the flux waveform by the search coil (Fig. 6 (b)) may be regarded as the air gap flux density distribution at no-load. If the winding coefficient K is multiplied on the flux, the third harmonic decreases by 10.9%, the fifth harmonic by 0.3% and the

seventh harmonic 0.04%. Therefore, an almost perfect sinusoidal induced emf can be obtained, as shown in Fig. 6 (c).

In this measurement, however, no influence by armature slots appears at all on the air gap flux waveform.

3.2 Derivation of Armature Reaction Flux

Fluxes cannot be combined or decomposed in the presence of saturation normally present in synchronous machines. Only mmf's can be so decomposed. But it would be very instructive for the physical understanding of the internal behavior of the synchronous machine to gain some knowledge of the shape and performance of armature reaction fluxes.

This section describes the derivation of armature reaction fluxes at various load power factors out of air gap fluxes on load, which are obtainable by means of a search coil. This can be done only when we neglect saturation effects. Operating the generator at a rated speed and connecting it to the load device, the air gap flux $\dot{\phi}$ is measured through the search coil No. 7 when the load power factor is changed ($\cos\varphi$). Also, the field flux $\dot{\phi}_f$ at no-load with the prescribed field current is to be measured. When subtracting $\dot{\phi}_f$ from $\dot{\phi}$ in conformity with the position of the direct axis, the armature reaction flux $\dot{\phi}_a$ may be found.

One of the examples is shown in Fig. 7 and Table 2. In this example, the field current 3.23 A and the armature current 10 A are both constant. From this illustration (Fig. 7 (a)), those armature reaction phenomena such as demagnetization, cross magnetization and magnetization can be visually grasped, with the power factor ($\cos\theta$) varied from lagging to leading. From Table 2, it may be found that as the result of the armature reaction, the armature terminal voltages decrease and increase as compared with no-load voltage (220 V, No. 0).

Table 2 also shows the results of the Fourier analysis with respect to waveforms as shown in Fig. 7 (a). With the internal power factor ($\cos\theta$) varied from leading to lagging, the fundamental wave component decreases and the harmonic components increases. Variations of these fundamental wave components are almost proportional to those of the armature terminal voltages.

When the field flux $\dot{\phi}_f$ (Fig. 7, No. 0) at no-load is subtracted from the air gap flux $\dot{\phi}$ on load from No. 1 through 11, shown in Fig. 7 (a), in conformity with the position of the direct axis, the armature reaction flux $\dot{\phi}_a$ can be found as shown in Fig. 7 (b). Because the generator is of a salient-pole machine type, the permeance between magnetic poles is small, and the magnetic flux becomes less there, so that pitting waveforms are seen between poles.

Variations versus the power factor angle θ of ϕ_{ad} (direct axis component of $\dot{\phi}_a$) and

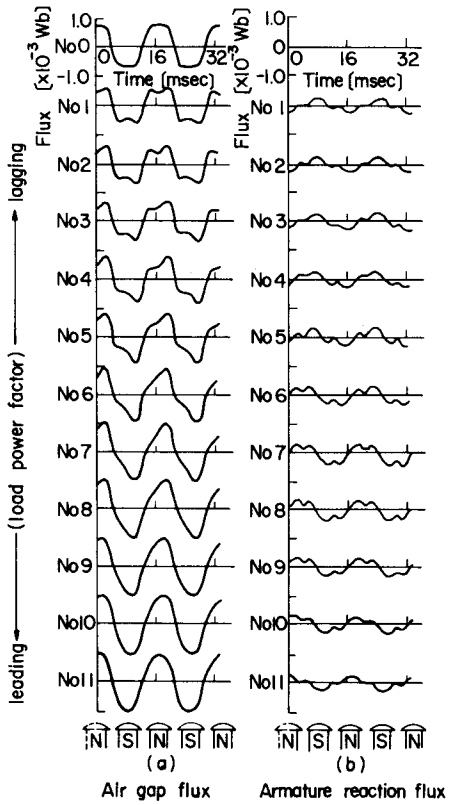

Fig. 7 Air gap flux and armature reaction flux waveforms at various load power factors

Table 2 Results of the Fourier analysis of search coil flux waveforms at various load power factors

No	Power factor		Phase angle	Terminal voltage	Fundamental component of ϕ	Harmonics/Fundamental %	
		cos φ	θ(°)	[V]	[×10⁻³ Wb]	3rd	5th
0		–	–	220	0.84	18.3	2.5
1		0.12	84	160	0.63	37.4	7.4
2	lagging ↑	0.30	77	161	0.63	36.7	7.4
3	lagging	0.50	68	166	0.64	35.7	7.7
4	lagging	0.71	63	175	0.70	33.1	6.9
5	lagging	0.90	44	188	0.74	30.5	7.7
6		1.00	24	210	0.82	25.5	6.9
7	leading	0.93	2	236	0.93	20.3	6.4
8	leading	0.76	-19	255	0.98	16.3	5.5
9	leading	0.51	-41	267	1.02	12.7	4.3
10	leading ↓	0.33	-58	272	1.04	10.1	3.3
11		0.12	-81	276	1.06	7.8	1.7

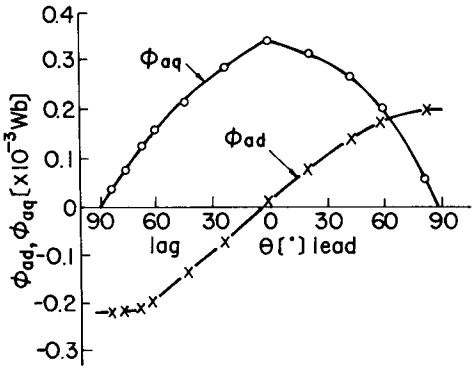

Fig. 8 Armature reaction fluxes ϕ_{ad} & ϕ_{aq} vs. θ

ϕ_{aq} (quadrature axis component of $\dot{\phi}_a$) are shown in Fig. 8. The component flux ϕ_{ad} is going to vary from negative to positive as the power factor angle (θ) varies from lagging to leading. On the other hand, the component flux ϕ_{aq} becomes maximum at the vicinity of $\theta=0°$. This indicates that the armature reaction appears as phenomena such as demagnetization, cross magnetization and magnetization in accordance with a variation of θ.

4 ANALYSIS OF LOSS OF SYNCHRONISM PROCESS

Power system stability essentially depends upon the loss of synchronism phenomena of a synchronous generator in the system. The phenomena arise when the torque supplied by the driving motor exceeds the electromagnetic torque exerted on the rotor shaft which is produced by the vector product of $\dot{\phi}_f$ and $\dot{\phi}_a$. Since it has been very difficult to analyze the phenomena physically, stability has so far been discussed by the internal phase differences between generators. This is the first time that the physical analysis of loss of synchronism process from the viewpoint of the internal behavior of the air gap flux has been successfully made clear. In this section, the air gap flux at the steady state is examined first, and then the loss of synchronism process due to a load increase is analyzed. The tested one-machine connected to an infinite bus system consists of the synchronous generator mentioned above, two transformers, a 3300 V transmission line and a 220 V three-phase power supply.

4.1 Air Gap Flux Waveform at the Steady State

Fig. 9 shows an air gap flux waveform by means of the search coil when no-load terminal voltage 230 V is generated at a rated speed. The zero point of time is arranged at a direct axis position. The air gap flux waveform is composed of odd

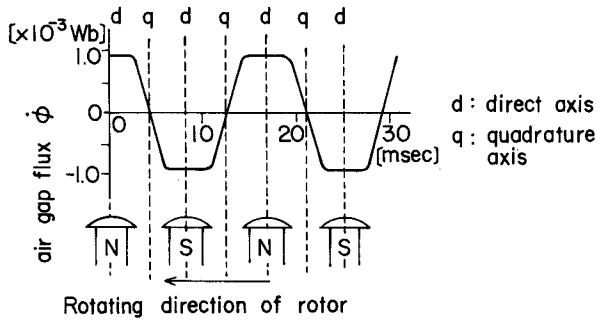

Fig. 9 Air gap flux waveform and pole position at no-load

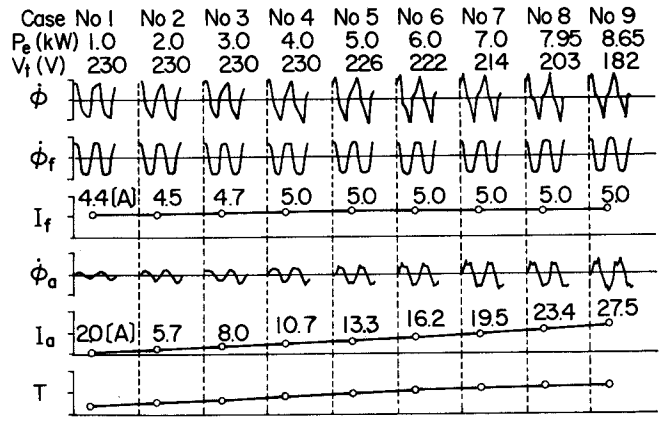

Fig. 10 Air gap flux, armature reaction flux, field current, torque, etc. at the steady state load condition (Test cases from No. 1 to No. 9)

harmonic components in a trapezoidal type due to the salient pole. It is of a symmetrical waveform in relation to the direct axis.

Next, Fig. 10 shows variations of air gap flux waveforms, field current, armature current and torque in cases where the output power Pe was increased by degrees after connecting the generator to the infinite-bus system. (Test Cases from No. 1 to No.9) The field current I_f produces the field flux $\dot{\phi}_f$, as shown in this figure. The armature reaction flux $\dot{\phi}_a$ increases with the armature current I_a. The torque acting on the rotor in the air gap is calculated as proportional to the vector products between $\dot{\phi}_f$ and $\dot{\phi}_a$ in every test case, as is shown in Fig. 10. This torque is balanced with the torque supplied by the driving motor in every test case to maintain synchronism.

In regard to the test case No. 9 of Fig. 10 the relationship between the air gap flux $\dot{\phi}$ and the pole position is shown in enlarged form in Fig. 11. This figure indicates

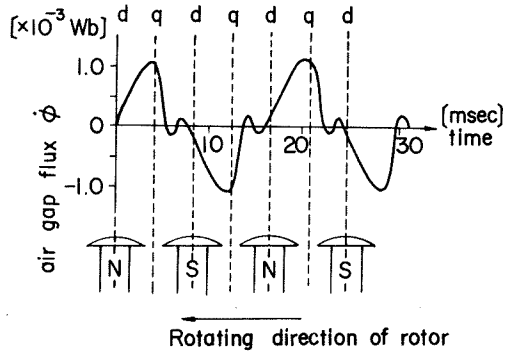

Fig. 11 Air gap flux waveform and pole position on load at the test case No. 9 of Fig. 10

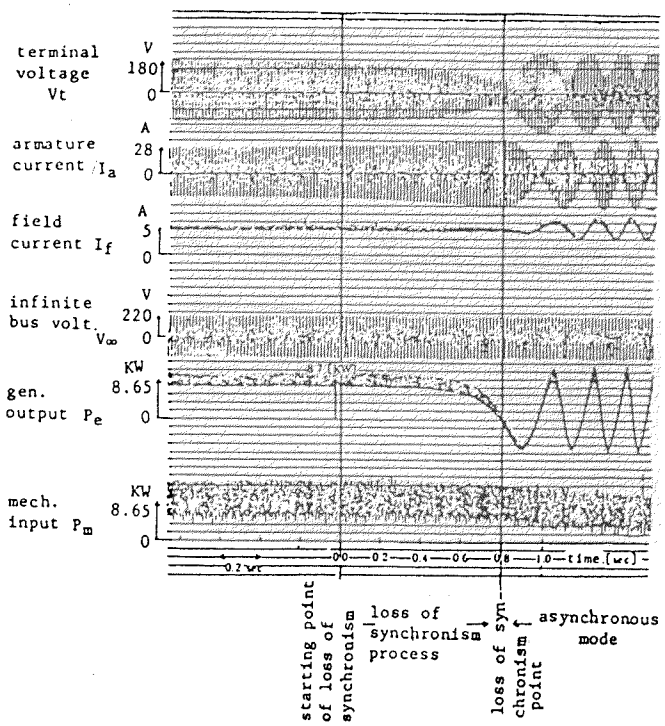

Fig. 12 Oscillograms of terminal voltage, armature current, etc., at the loss of synchronism process

that air gap flux waveforms ϕ are gradually distorted compared with those at no-load (see Fig. 9) by the armature reaction, with an increase of the load current, and the flux at the center of magnetic pole is extremely lessened. Thus, the flux is concentrated at the lagging side of the pole surface.

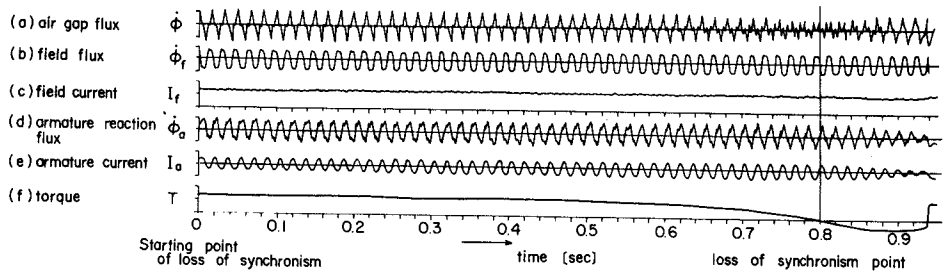

Fig. 13 Changes of air gap flux, ar mature reaction flux, etc., at the loss of synchronism process

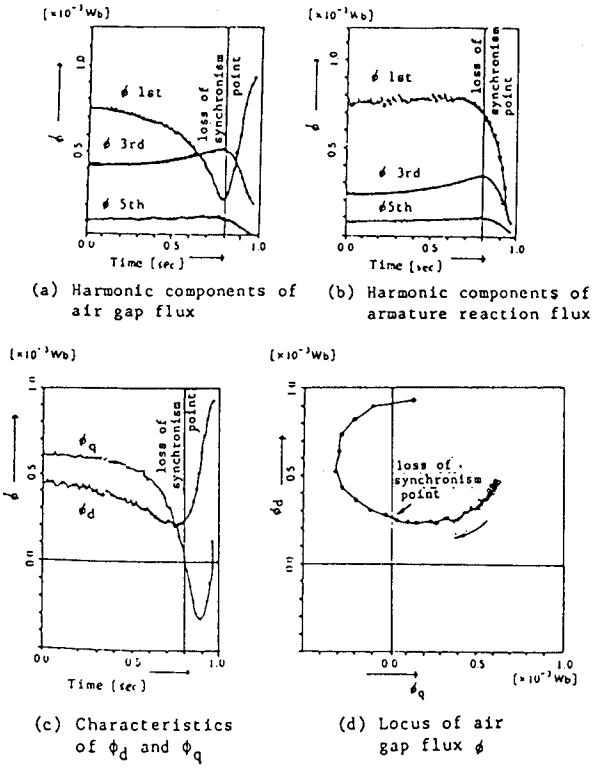

Fig. 14 Flux characteristics at the loss of synchronism process

These phenomena show that the direct axis component of $\dot{\phi}$ decreases while its quadrature axis component increases the other way, with an increase of the load current. The reason for this is clear from the phasor diagram in Fig. 2, where the lagging phase angle θ increases with the load current. Consequently, the flux produced by the field current decreases due to the demagnetization effect of the lagging armature current. And the quadrature axis component of $\dot{\phi}$ increases due to

the increase of the active component ($I_a \cos \theta$) of the armature current.

4.2 Loss of Synchronism Process

In the case of No. 9, Fig. 10, the generator delivers an output power of 8.65 kW. If the driving power is increased further with the constant field current 5 A, the output power of the generator increases up to 8.7 kW, but then begins to decrease and the rotor speed begins to increase. We determined that the generator enters the loss of synchronism process when the rotor speed begins to increase. Fig. 12 shows oscillograms of the terminal voltage, armature current, generator output, mechanical input, etc. at the loss of synchronism process.

The generator becomes out-of-step completely when Pe = 0. At this loss of synchronism point, the terminal voltage V_t takes a minimum value and the armature current I_a takes a maximum value. This fact can be utilized in detecing the loss of synchronism point. The air gap flux, field current, armature reaction flux, armature current and torque are illustrated in Fig. 13.

The curves in Fig. 14 (a) and (b) indicate how the fundamental and the harmonic components of the air gap flux $\dot{\phi}$ and the armature reaction flux $\dot{\phi}_a$, as shown in Fig. 13, vary with time respectively. The curves in Fig. 14 (c) and (d) also show how the direct axis component ϕ_d of $\dot{\phi}$ and the quadrature axis component ϕ_q of $\dot{\phi}$ vary with time. Measured data of these curves have been obtained by measuring them each time the rotor rotates by a one-half turn.

From these figures, we can draw the following conclusions.

(1) After the staring point of the loss of the synchronism process, the waveform of $\dot{\phi}_f$ continues to be of a trapezoidal form, and it rotates at the same speed as the rotor. By contrast, the waveform of $\dot{\phi}_a$ changes with the magnitude and frequency of the armature current, as shown in Fig. 13. Torque T, derived from $\dot{\phi}_f$ and $\dot{\phi}_a$, continues to decrease and vanishes at the loss of synchronism point.

(2) After the starting point of the loss of synchronism process, the fundamental component of the air gap flux $\dot{\phi}$ decreases with time, and the third and fifth harmonic components increase. At the loss of synchronism point, the fundamental component takes a minimum value, and both the third and fifth harmonic components take maximum value. This phenomenon is caused by the increase of the lagging phase angle due to the acceleration of the rotor. This fact can be utilized to detect the loss of synchronism point.

(3) Although the fundamental component of the armature reaction flux $\dot{\phi}_a$ changes to a considerable extent at the loss of synchronism point, it cannot be used to detect this point. The third and fifth harmonic components take

maximum value at this point.

(4) Although ϕ_d is located somewhere near the minimum value at the loss of synchronism point, ϕ_q vanishes at this point. Therefore, this point can be detected by measuring the vanishing point of ϕ_q.

5 CONCLUSION

Using a 6 kVA synchronous generator, the characteristics of a synchronous generator have been analyzed by air gap fluxes measured by a search coil wound around a tooth top of the stator. It was the first time that the loss of synchronism phenomena was thus made clear.

These analyses will assist us in gaining a physical understanding of the inrernal behavior of a synchronous machine. They will also contribute to both machine designs and power system stability studies.

6 ACKNOWLEDGEMENT

The authors would like to thank Emeritus Professor Chikasa Uenosono of Kyoto University for his continuous support and encourgement. This research was supported by Grant-in-Aid for Scientific Research from the Ministry of Education, Science and Culture of Japan.

REFERENCES

1) C.Uenosono, J.Matsuki and T.Okada, "Analysis of steady-state characteristics of salient-pole synchronous generator by flux waveforms detected by search coils" , EEIJ, Vol.99, No.3, 1979, pp.371-378.
2) C.Uenosono, J.Matsuki and T.Okada, "Analysis of step-out process of a three-phase synchronous machine by air gap fluxes," EEIJ, Vol.100, No.1, 1980, pp.41-48.
3) P.Silvester and M.V.K.Chari, "Finite element solution of saturable magnetic field problems," IEEE Transactions on Power Apparatus and Systems, PAS, Vol.89, 1970, pp.1642-1651.
4) S.V.Ahamed and E.A.Erdélyi, "Nonlinear theory of salient pole machines," IEEE transactions on Power Apparatus and Systems, PAS, Vol.85, 1966, pp.61-70.
5) R.W.Wieseman, "Graphical determination of magnetic fields," Trans. AIEE, Vol.44, 1927, pp.141-151.
6) N.A.Demerdash, V.K.Garg and H.B.Hamilton, "Effect of ventilating holes on radial flux and losses in stator slots of turbogenerators," IEEE Transactions on Power Appratus and Systems, PAS, Vol.94, 1975, pp.1177-1182.